Synthesis, luminescence, and electrochemical studies of a tetra- and an octanuclear ruthenium(II) complexes of tolylterpyridine appended calixarenes

Selvam Amudhan Senthan and Vedamanickam Alexander*
Department of Chemistry, Loyola College, Chennai-600034, India.

Electronic supplementary information

New Journal of Chemistry

Table of Contents

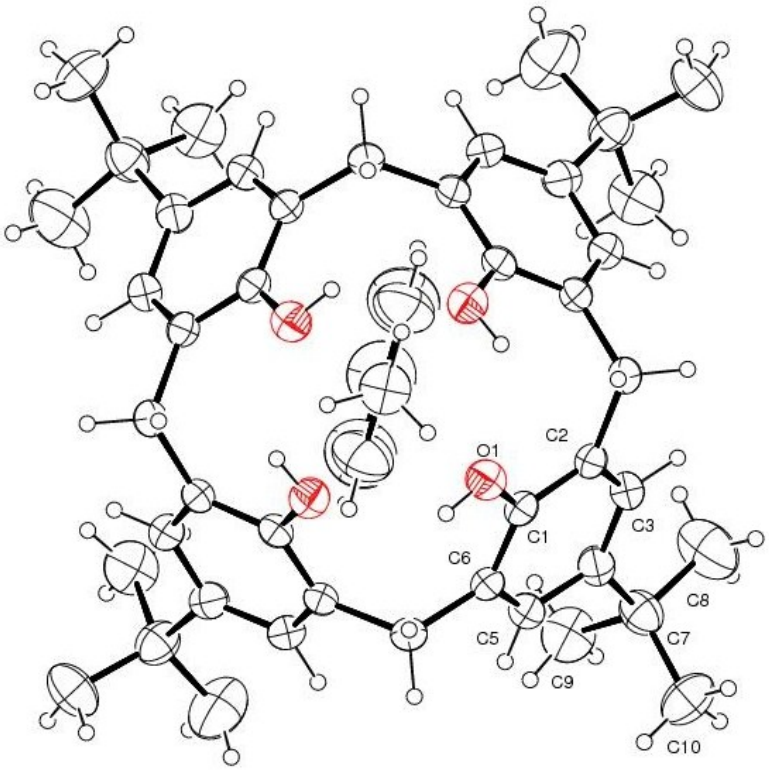

Figure S1. ORTEP representation of **1** with atoms represented as 35% probability thermal ellipsoids.

Table S1. The crystal structure data of 5,11,17,23-tetra-*tert*-butyl-25,26,27,28-tetrahydroxy-calix[4]arene (1)

Description	**1**
empirical formula	$C_{51}H_{64}O_4$
formula weight	741.02
T, K	293(2)
λ, Å	0.71073
crystal system	tetragonal
space group	$P4/n$
a, Å	12.754(5)
b, Å	12.754(5)
c, Å	13.787(6)
α, deg	90
β, deg	90
γ, deg	90
V, Å^3	2243(2)
Z	2
ρ_{calcd}, mg m^{-3}	1.097
absorption coefficient, mm^{-1}	0.067
F(0 0 0)	804
shape / colour	Block / colourless
θ range for data collection, deg	2.175 to 24.99
reflections collected / unique	21156 / 1990 [R(int) = 0.0281]
absorption correction	Semi-empirical from equivalents
max. and min. transmission	0.96 and 0.93
refinement method	Full-matrix least-squares on F^2
data/restraints/parameters	1990/154/184
goodness of fit on F^2	1.103
final R indices [$I > 2\sigma(I)$][a]	R1 = 0.0500, wR2 = 0.1381
R indices (all data) [a]	R1 = 0.0755, wR2 = 0.1722
Largest diff. peak and hole	0.188 and -0.250e Å^{-3}

[a] $R1 = \Sigma||F_o| - |F_c|| / \Sigma |F_o|$; $wR2 = [\Sigma\{w(F_o^2 - F_c^2)\}^2 / \Sigma\{wF_o^2)^2\}]^{1/2}$.

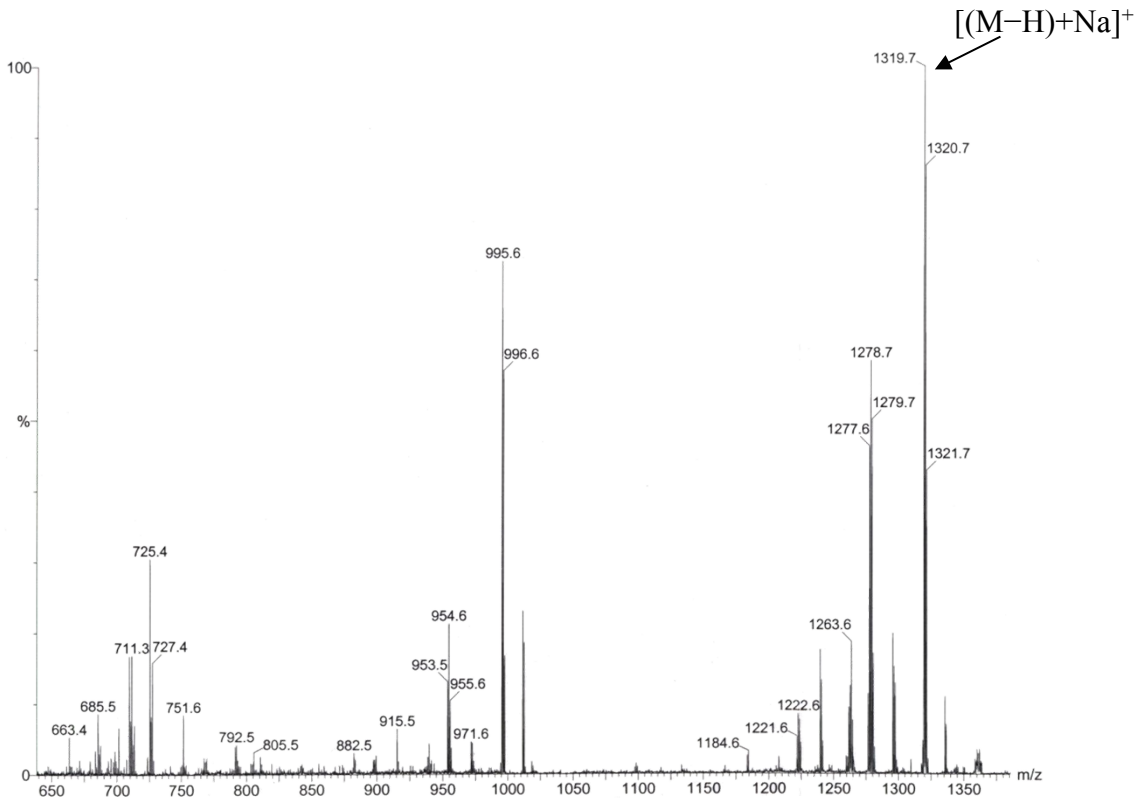

Figure S2. MALDI-TOF mass spectrum of 5,11,17,23,29,35,41,47-octa-*tert*-butyl-49,50,51,52,53, 54,55,56-octahydroxycalix[8]arene (**2**).

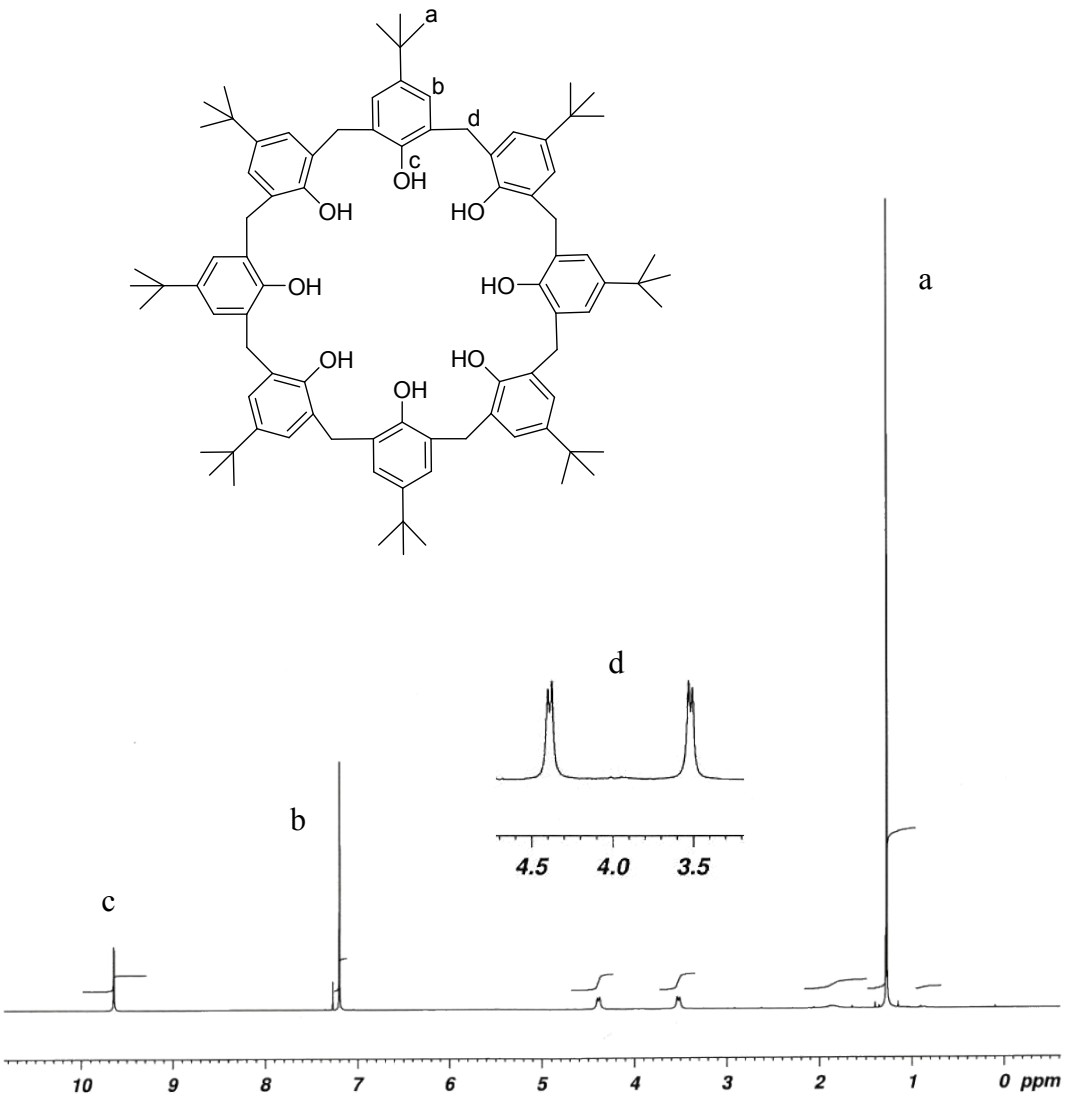

Figure S3. 500 MHz ^{1}H NMR spectrum of 5,11,17,23,29,35,41,47-octa-*tert*-butyl-49,50,51,52,53, 54, 55,56-octahydroxycalix[8]arene (**2**) in $CDCl_3$.

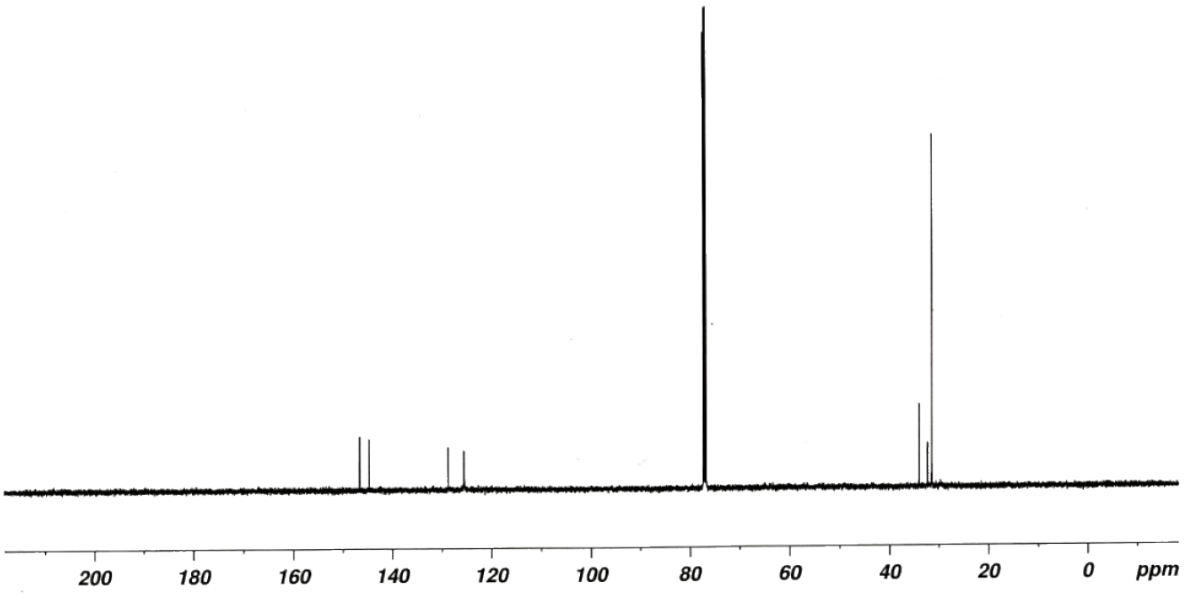

Figure S4. 125 MHz ^{13}C NMR spectrum of 5,11,17,23,29,35,41,47-octa-*tert*-butyl-49,50,51,52,53, 54, 55,56-octahydroxycalix[8]arene (**2**) in $CDCl_3$.

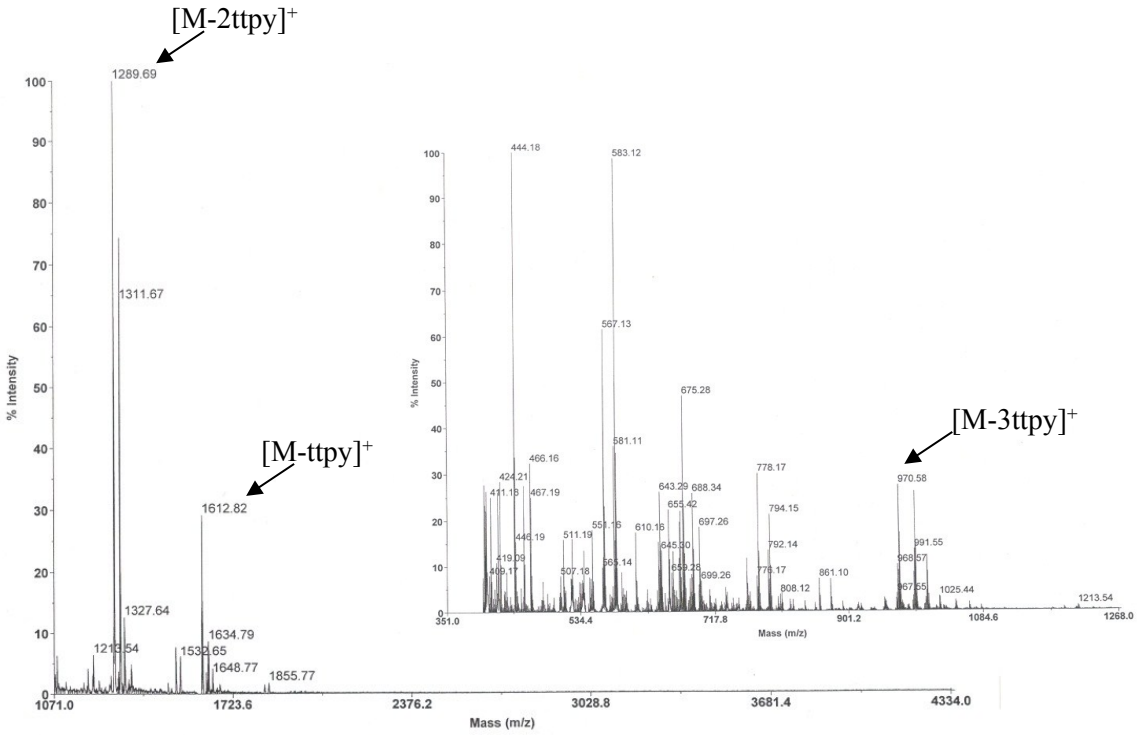

Figure S5. MALDI-TOF mass spectrum of 5,11,17,23-tetra-*tert*-butyl-25,26,27,28-tetra(4′-*p*-benzyl-oxy-(2,2′:6′,2″-terpyridinyl))calix[4]arene (**L^1**).

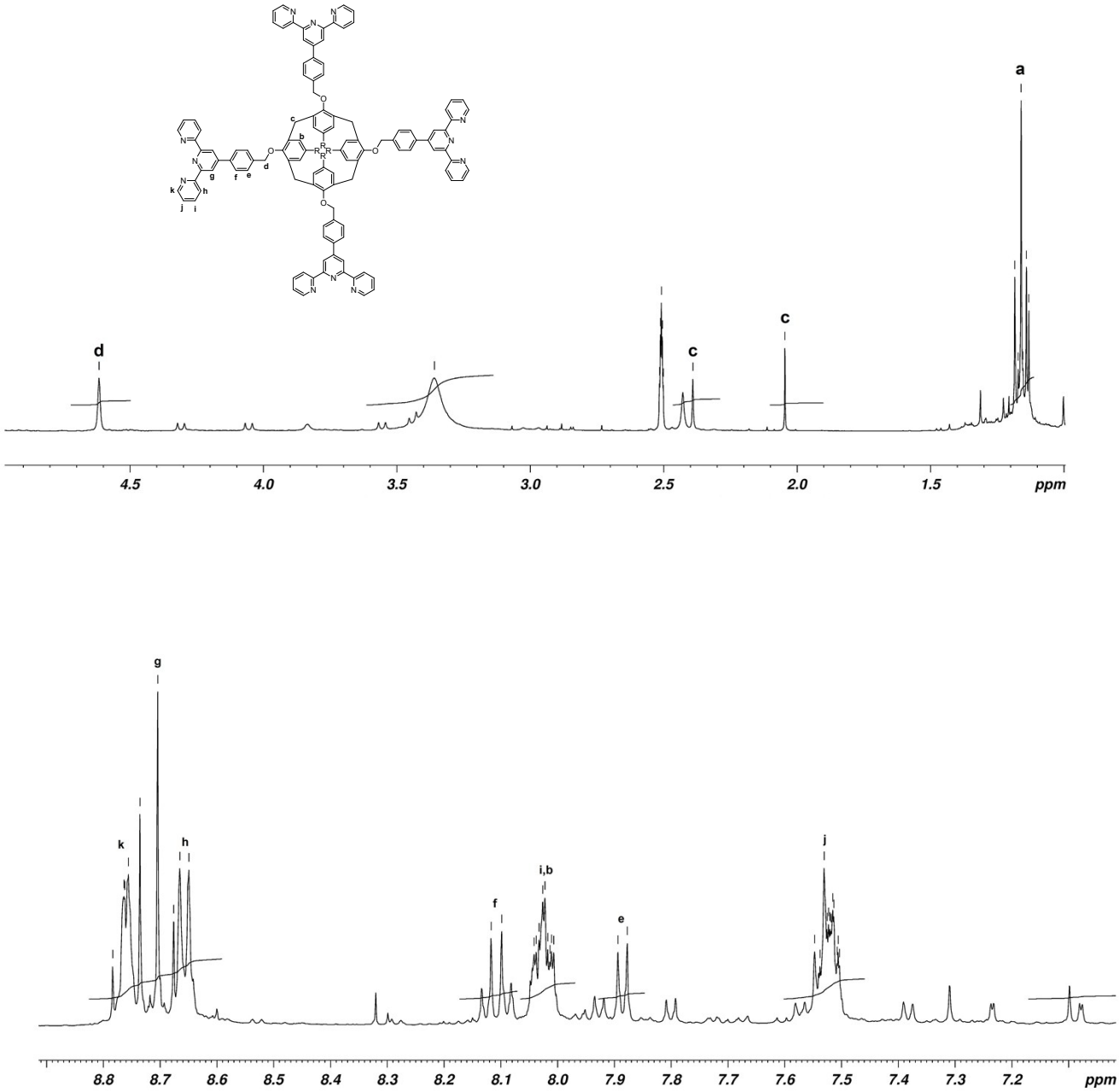

Figure S6. 500 MHz ^{1}H NMR spectrum of 5,11,17,23-tetra-*tert*-butyl-25,26,27,28-tetra(4′-*p*-benzyl-oxy-(2,2′:6′,2″-terpyridinyl))calix[4]arene (**L^{1}**) in DMSO-d_6.

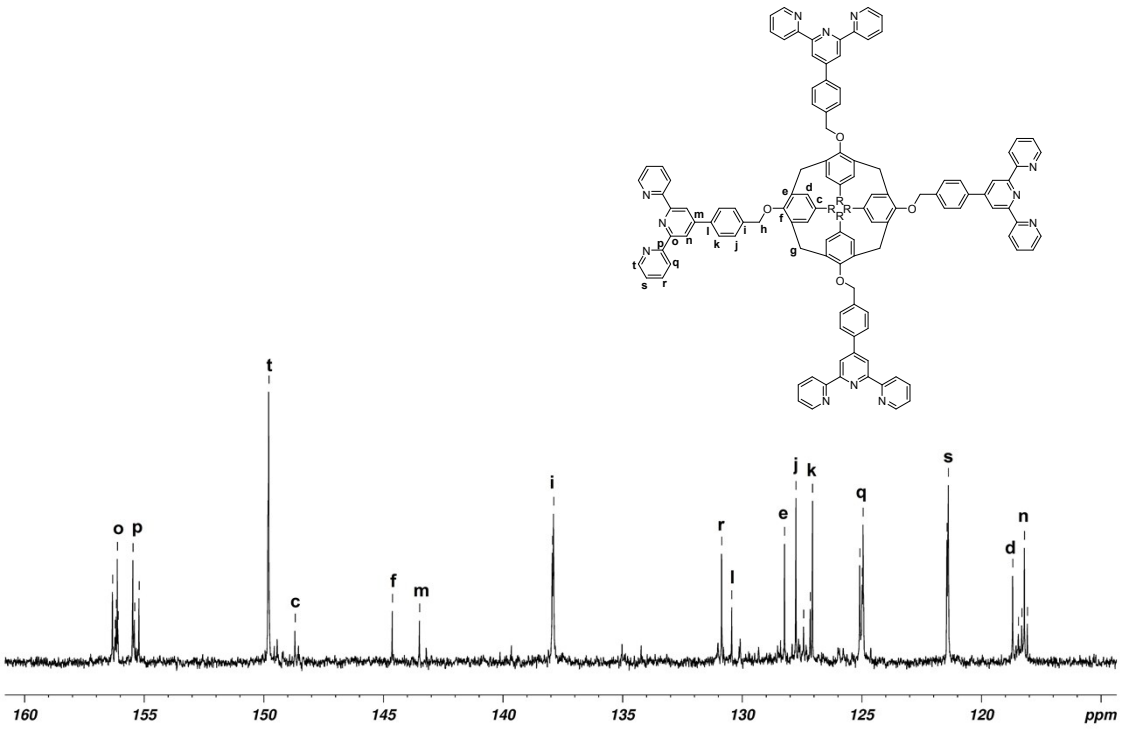

Figure S7. 125 MHz ^{13}C NMR spectrum of 5,11,17,23-tetra-*tert*-butyl-25,26,27,28-tetra(4′-*p*-benzyl-oxy-(2,2′:6′,2″-terpyridinyl))calix[4]arene (**L^{1}**) in DMSO-d_6.

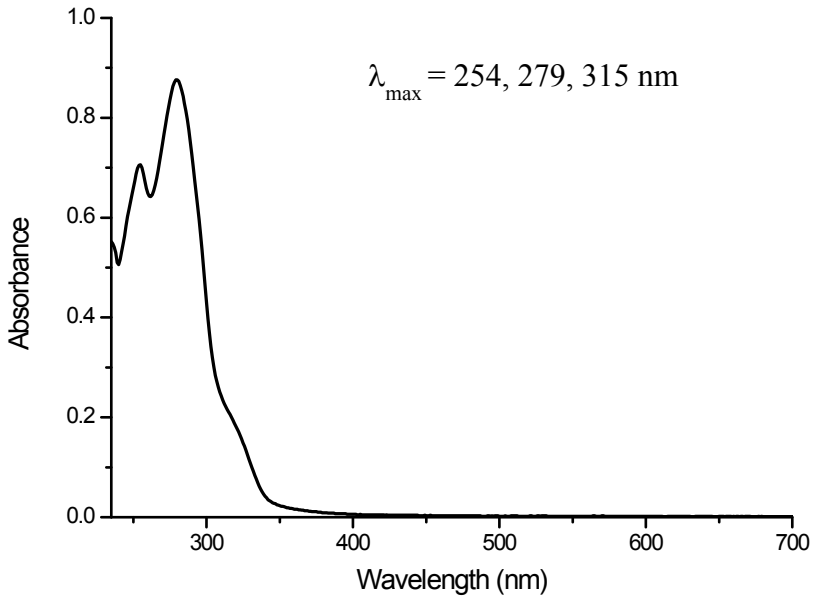

Figure S8. Electronic absorption spectrum of 5,11,17,23-tetra-*tert*-butyl-25,26,27,28-tetra(4′-*p*-benzyl-oxy-(2,2′:6′,2″-terpyridinyl))calix[4]arene (**L**^{1}) in $CHCl_3$ at 25 °C.

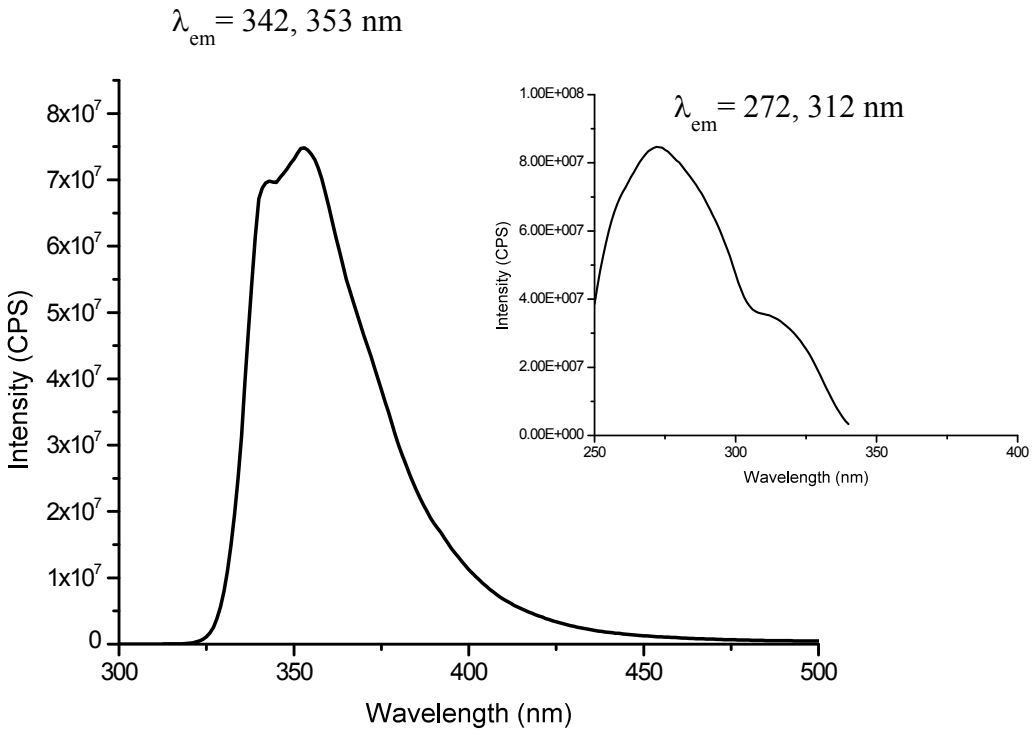

Figure S9. Emission spectrum of **L[1]** in $CHCl_3$ at 298 K (λ_{ex} = 272 nm); inset: excitation spectrum (λ_{em} = 342, 353 nm).

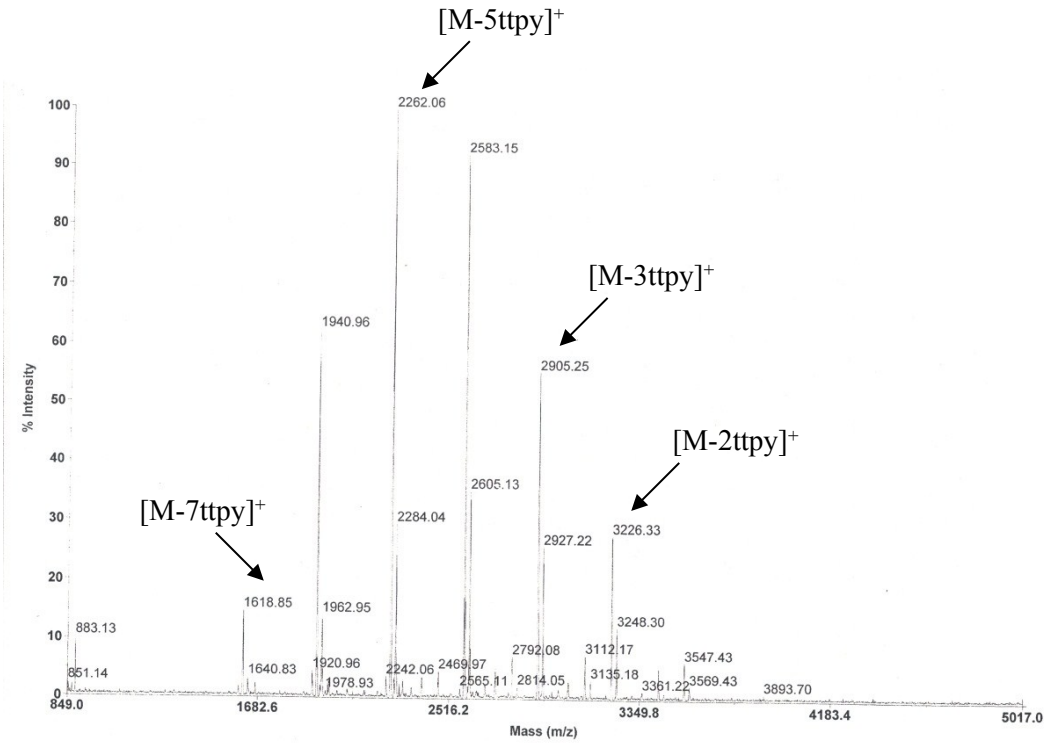

Figure S10. MALDI-TOF mass spectrum of 5,11,17,23,29,35,41,47-octa-*tert*-butyl-49,50,51,52,53,54, 55,56-octa(4′-*p*-benzyloxy-(2,2′:6′,2″-terpyridinyl))calix[8]arene (**L²**).

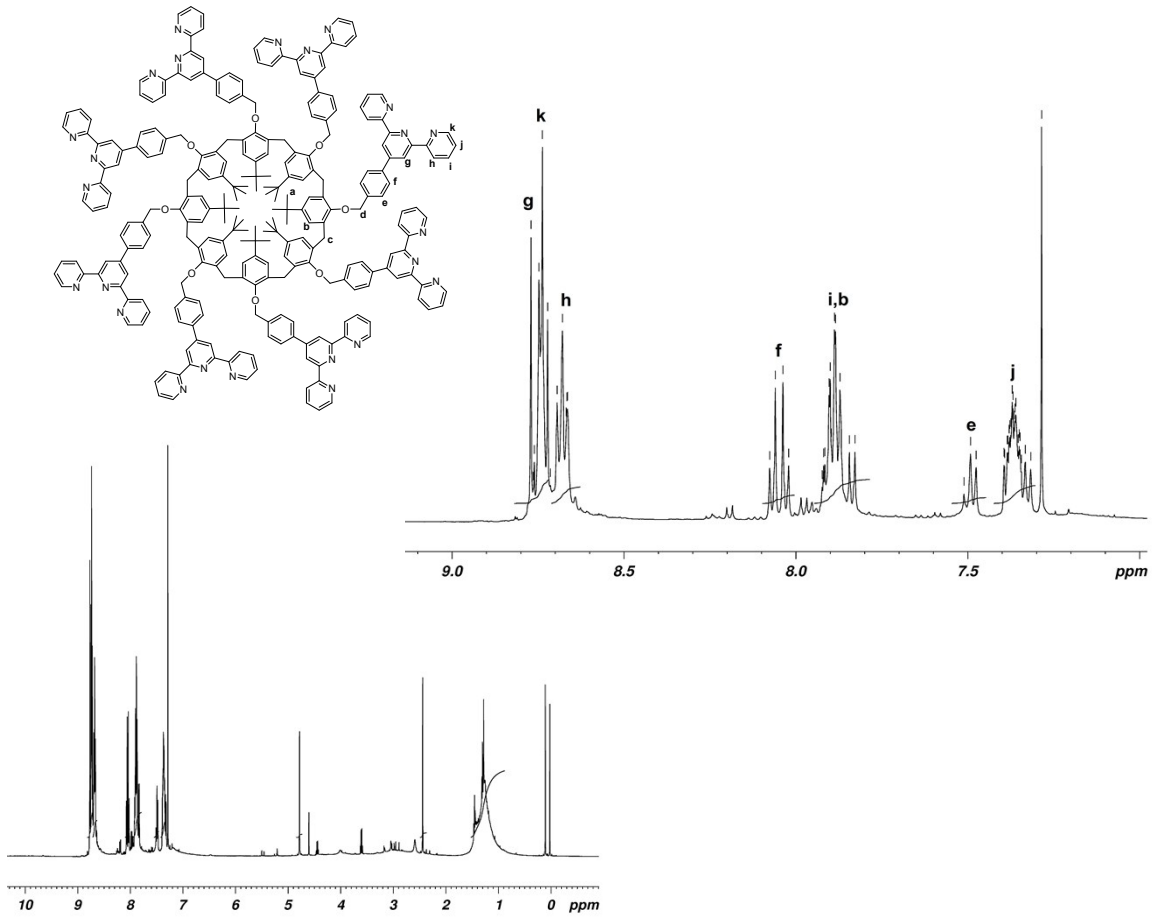

Figure S11. 500 MHz ^{1}H NMR spectrum of 5,11,17,23,29,35,41,47-octa-*tert*-butyl-49,50,51,52,53,54, 55,56-octa(4′-*p*-benzyloxy-(2,2′:6′,2″-terpyridinyl))calix[8]arene (**L²**) in $CDCl_3$.

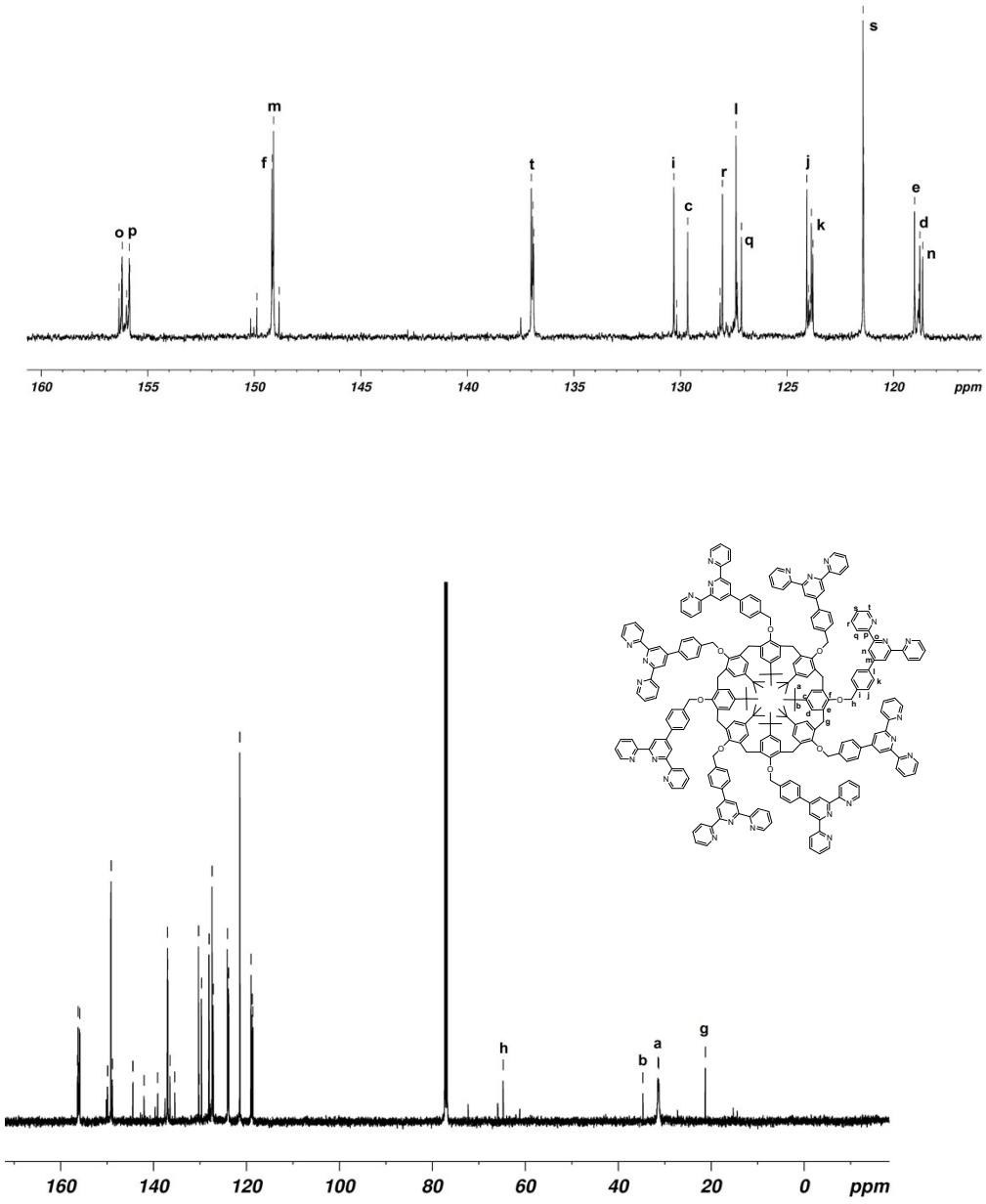

Figure S12. 125 MHz ^{13}C NMR spectrum of 5,11,17,23,29,35,41,47-octa-*tert*-butyl-49,50,51,52,53,54, 55,56-octa(4′-*p*-benzyloxy-(2,2′:6′,2″-terpyridinyl))calix[8]arene (**L²**) in $CDCl_3$.

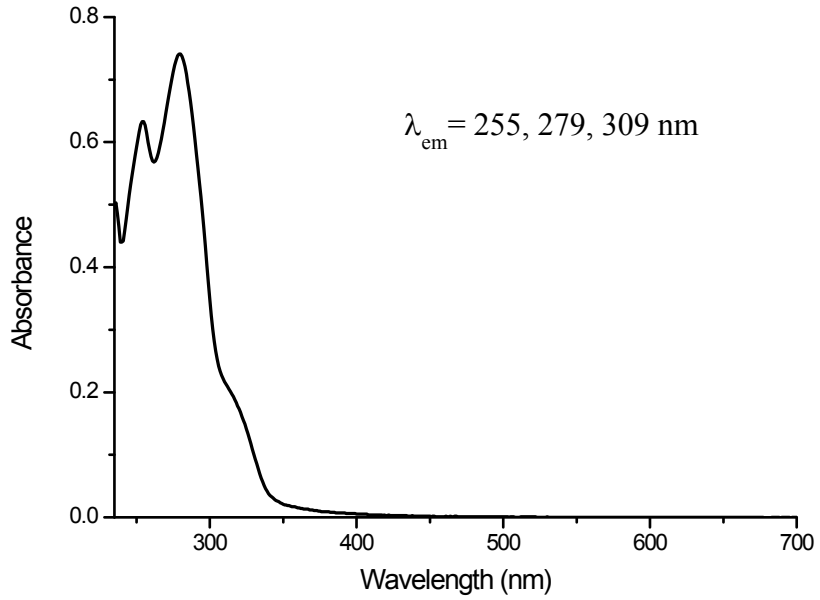

Figure S13. Electronic absorption spectrum of **L²** in $CHCl_3$ at 25 °C.

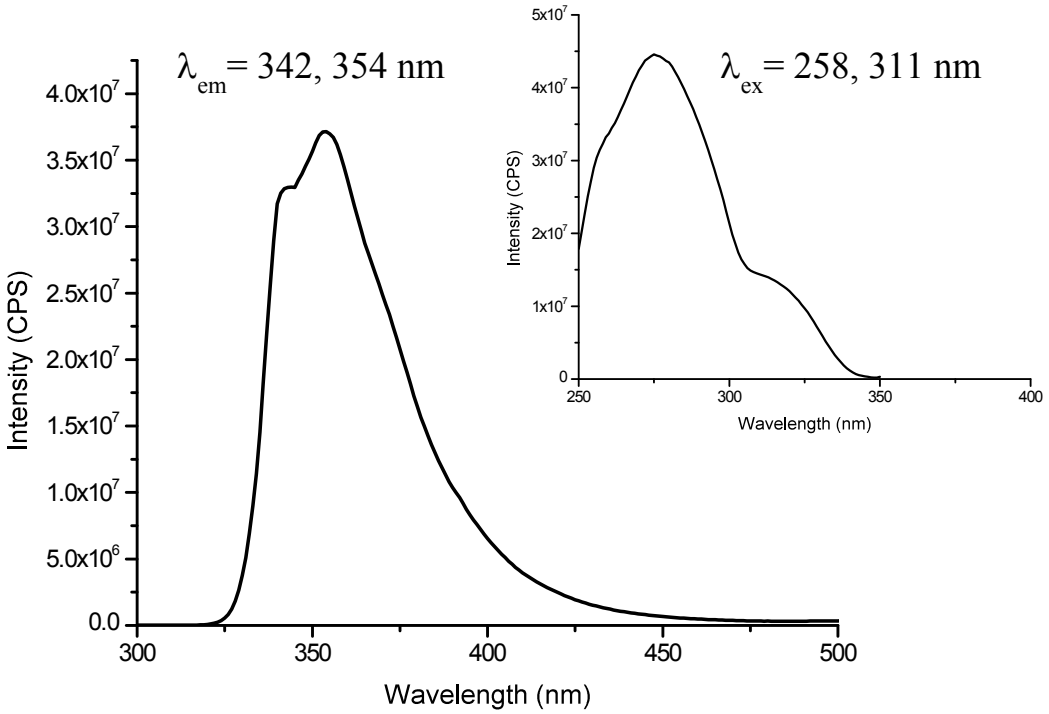

Figure S14. Emission spectrum of **L²** in $CHCl_3$ at 298 K (λ_{ex} = 275 nm), inset: excitation spectrum (λ_{em} = 342, 354 nm).

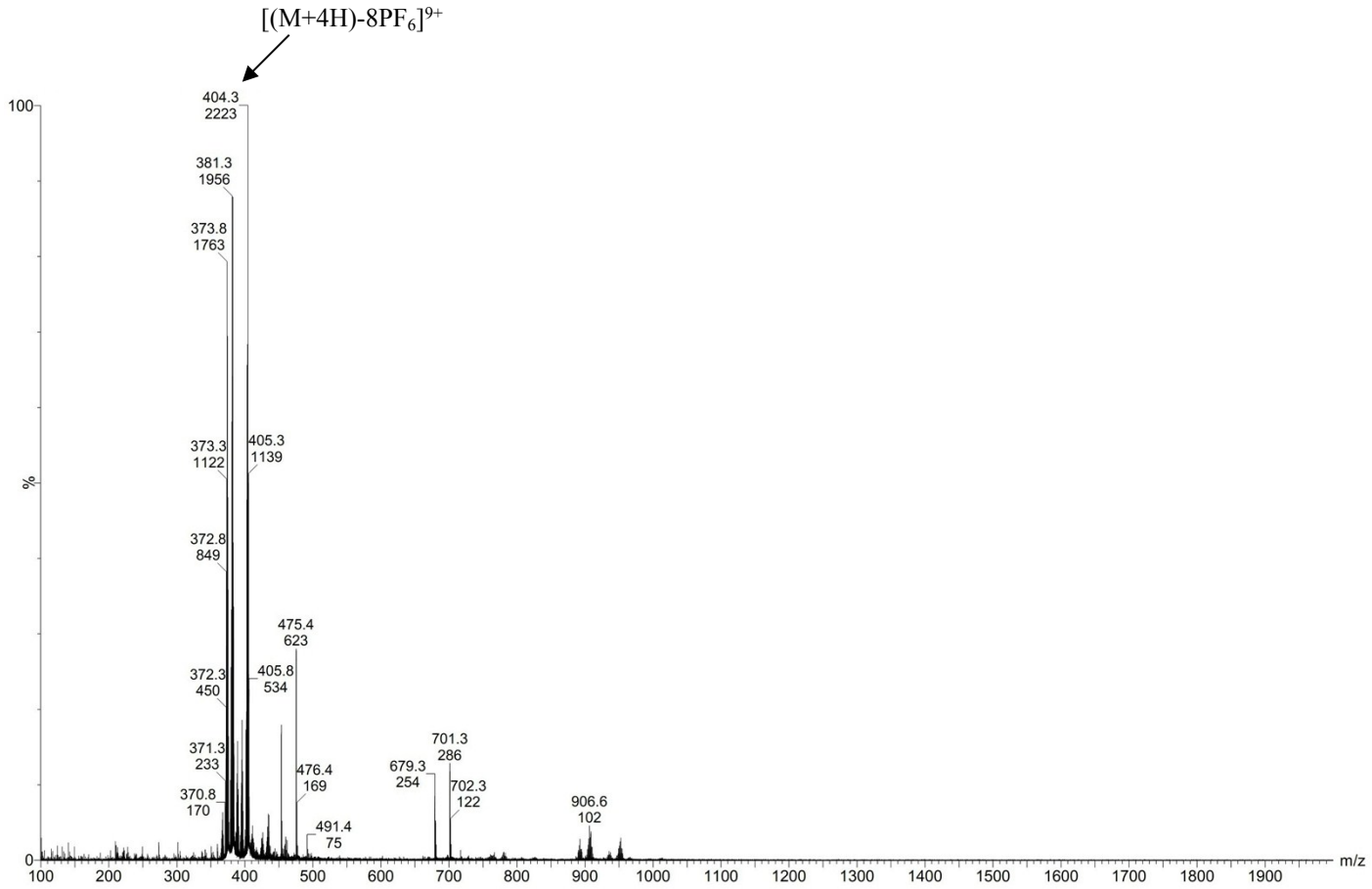

Figure S15. ESI-TOF mass spectrum of [{Ru(ttpy)}$_4$(**L^1**)](PF$_6$)$_8$ (**3**).

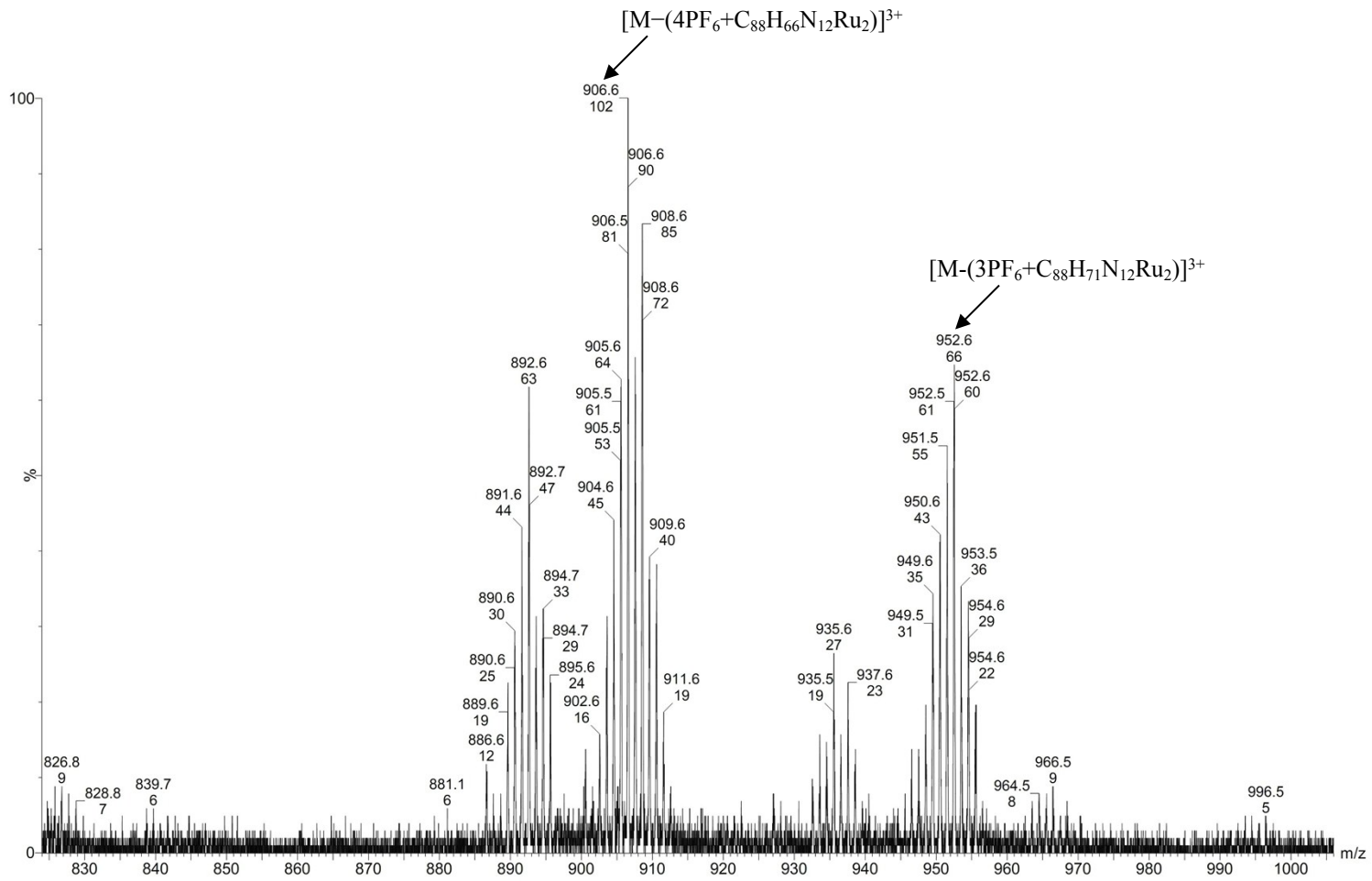

Figure S15a. ESI-TOF mass spectrum of [{Ru(ttpy)}$_4$(**L^1**)](PF$_6$)$_8$ (**3**) (expanded).

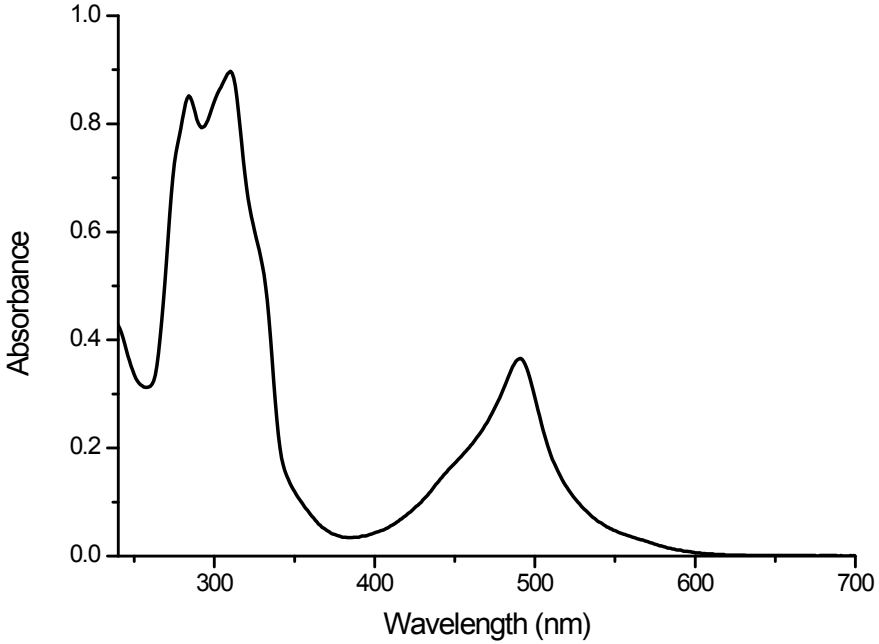

λ_{max} = 284, 309, 325, 490 nm

Figure S16. Electronic absorption spectrum of [{Ru(ttpy)}$_4$(**L1**)](PF$_6$)$_8$ (**3**) in CH_3CN at 25 °C.

λ_{em}= 663 nm λ_{ex}= 367, 464, 539 nm

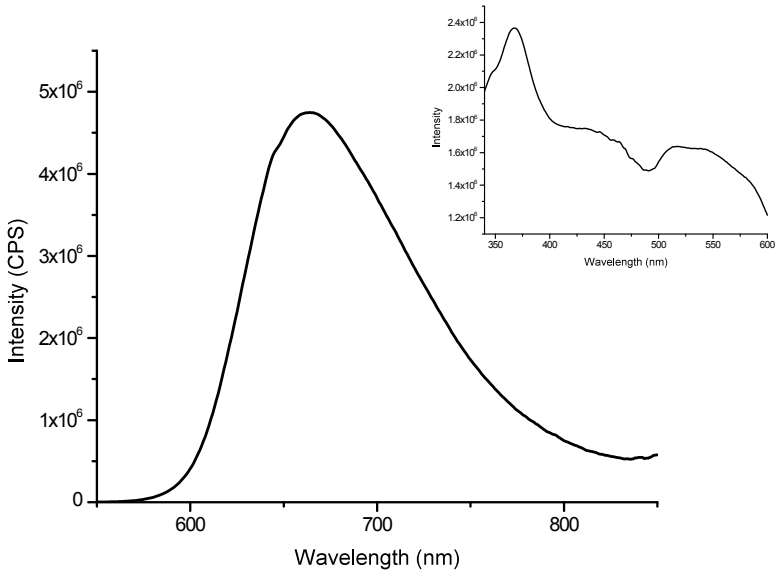

Figure S17. Emission spectrum of [{Ru(ttpy)}$_4$(**L^1**)](PF$_6$)$_8$ (**3**) in solid state at 25 °C, inset: excitation spectrum (λ_{ex}= 367 nm).

λ_{em}= 650, 690 nm

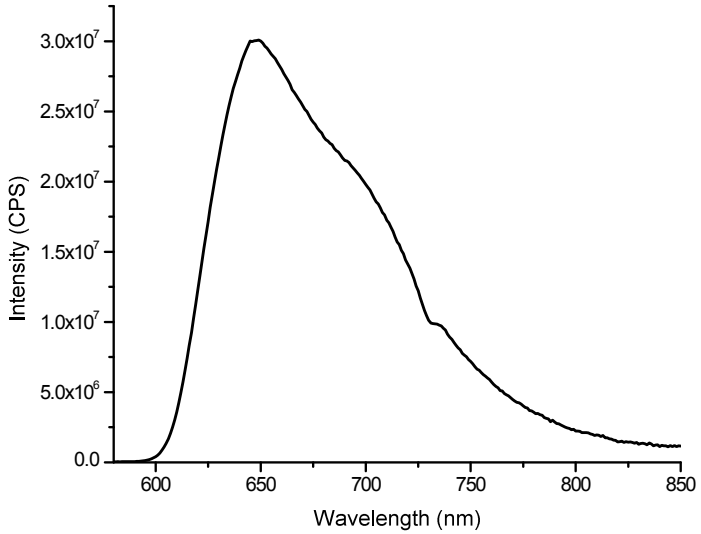

Figure S18. Emission spectrum of [{Ru(ttpy)}$_4$(**L^1**)](PF$_6$)$_8$ (**3**) in CH_3CN at 77 K.

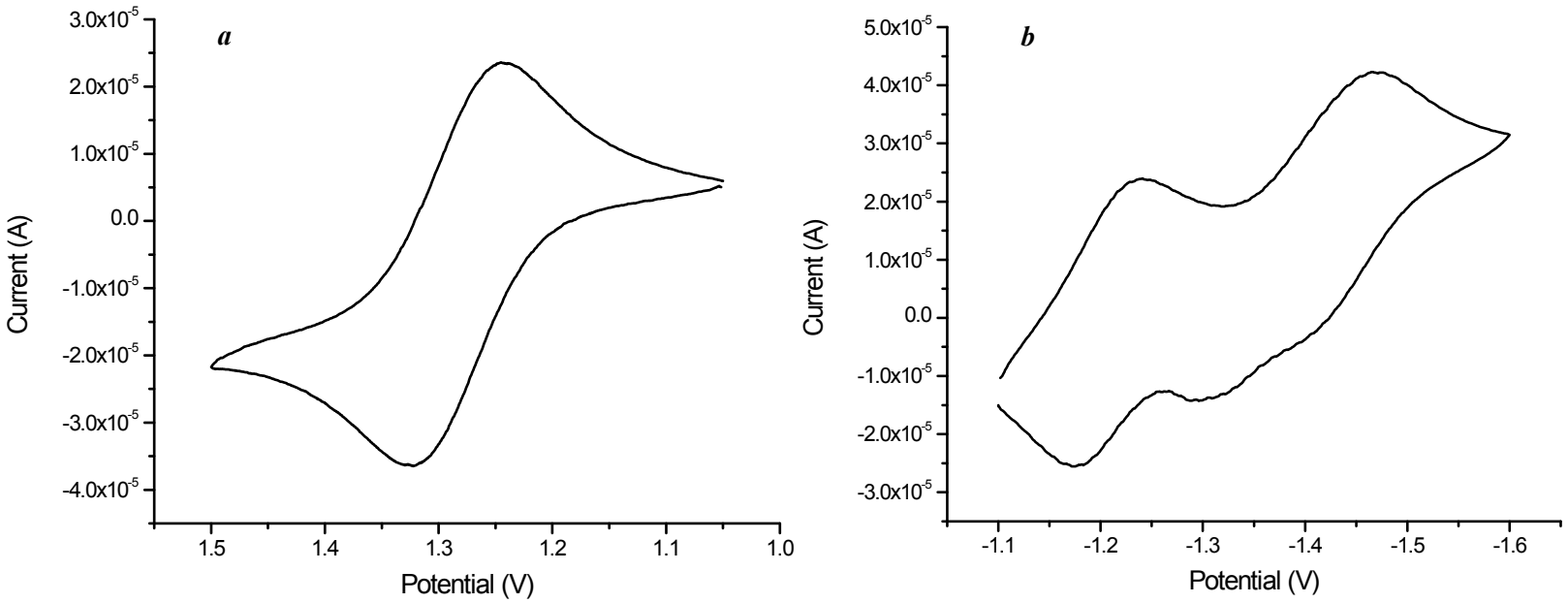

Figure S19. Cyclic voltammogram of $[\{Ru(ttpy)\}_4(\mathbf{L^1})](PF_6)_8$ (**3**) on a glassy carbon millielectrode in acetonitrile (0.1 M Et_4NClO_4) versus Ag/Ag^+ at 25 °C, scan rate = 50 mVs^{-1}, (*a*) positive potential and (*b*) negative potential window.

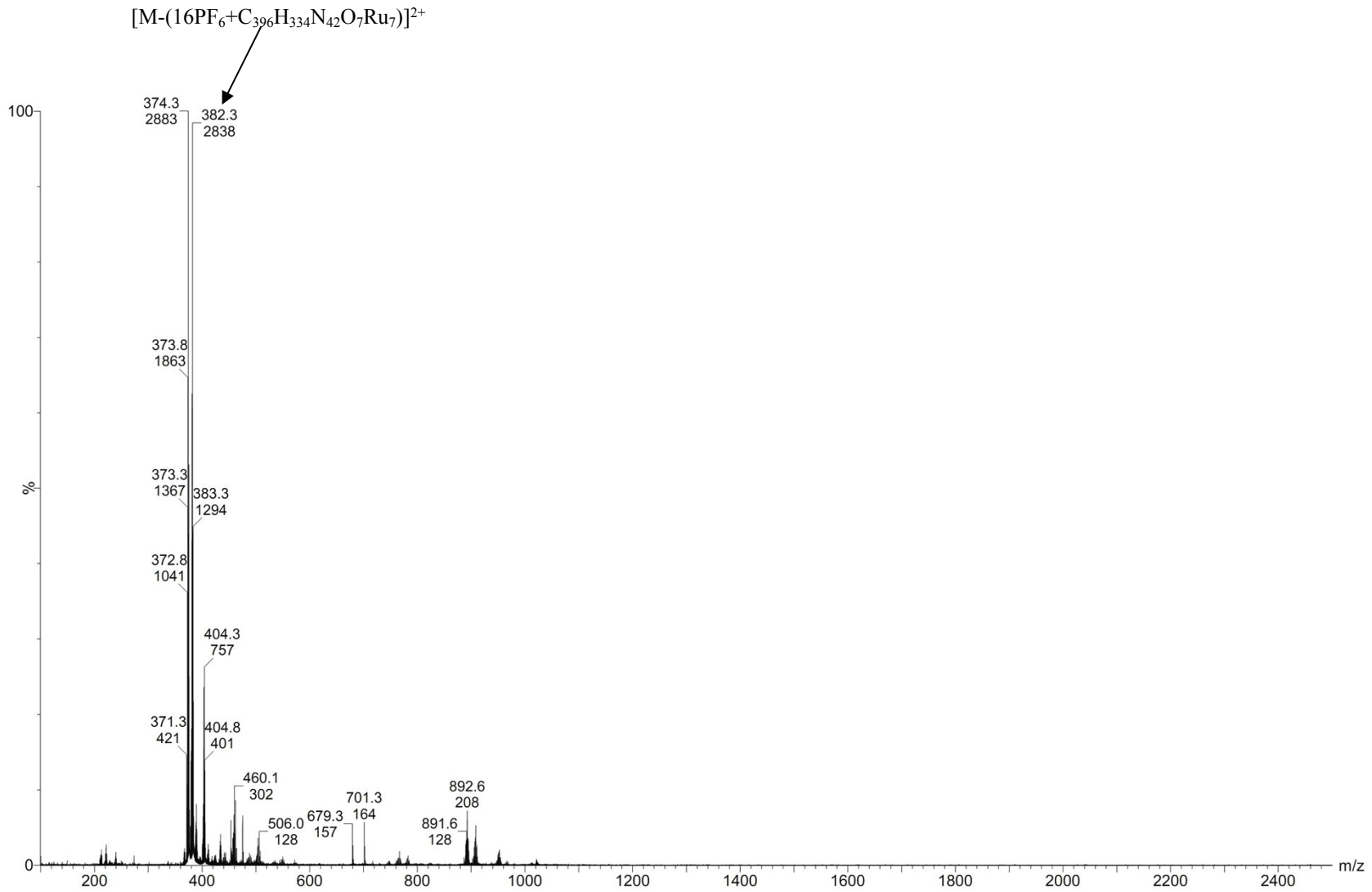

Figure S20. ESI-TOF mass spectrum of $[\{Ru(ttpy)\}_8(\mathbf{L^2})](PF_6)_{16}$ (**4**).

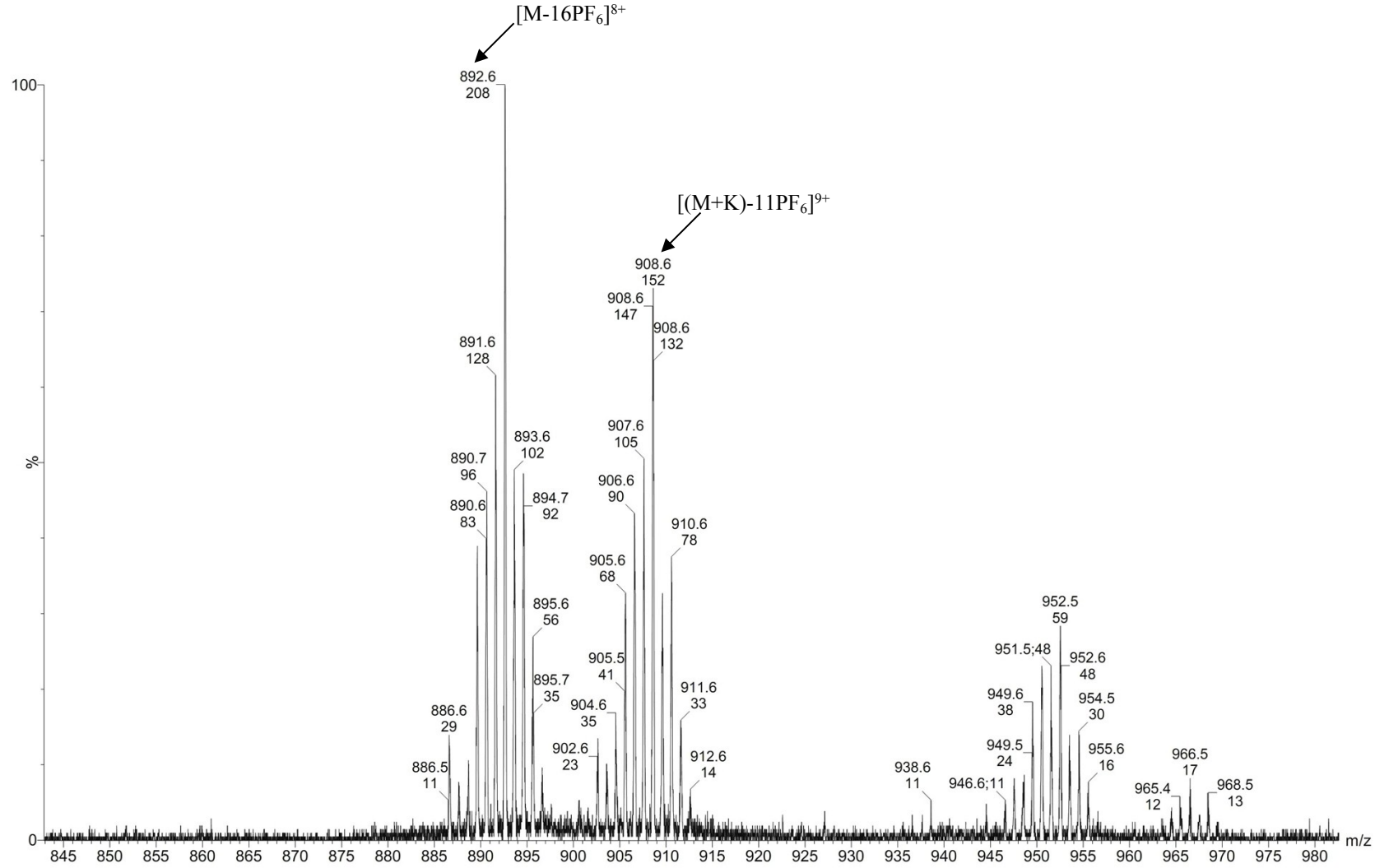

Figure S20a. ESI-TOF mass spectrum of [{Ru(ttpy)}$_8$(**L^2**)](PF$_6$)$_{16}$ (**4**) (expanded).

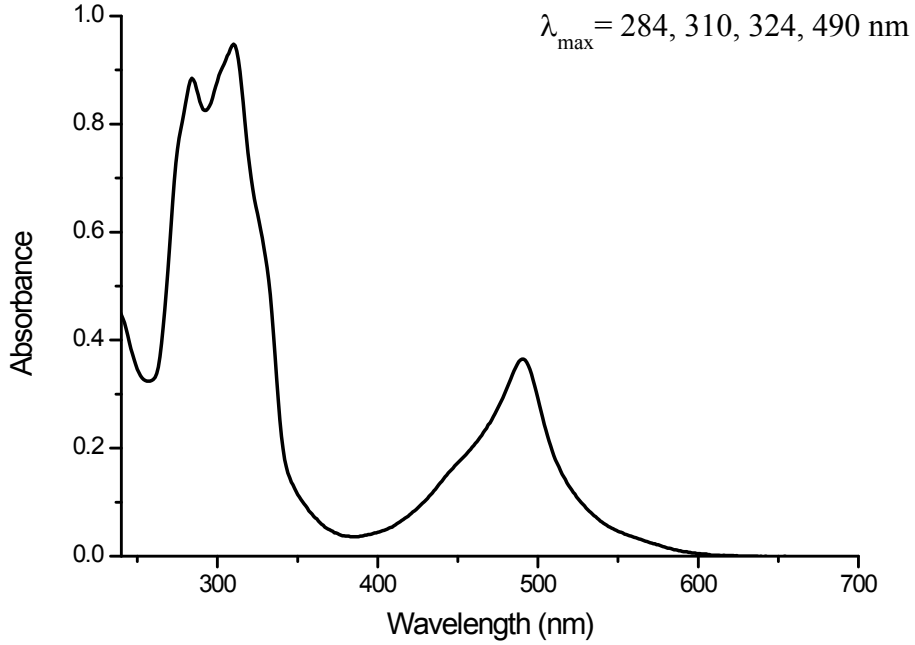

Figure S21. Electronic absorption spectrum of $[\{Ru(ttpy)\}_8(\mathbf{L^2})](PF_6)_{16}$ (**4**) in CH_3CN at 25 °C.

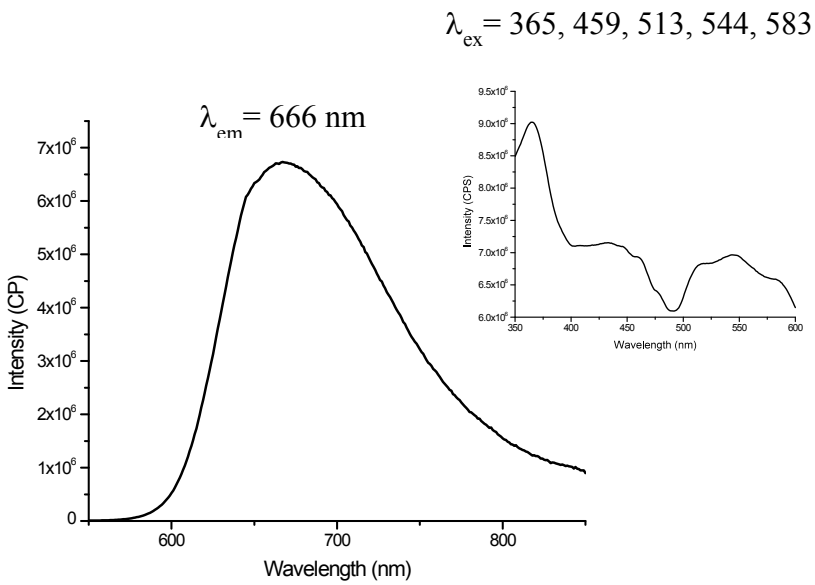

Figure S22. Emission spectrum of [{Ru(ttpy)}$_8$(**L^2**)](PF$_6$)$_{16}$ (**4**) in solid state at 25 °C, inset: excitation spectrum (λ_{ex}= 365 nm).

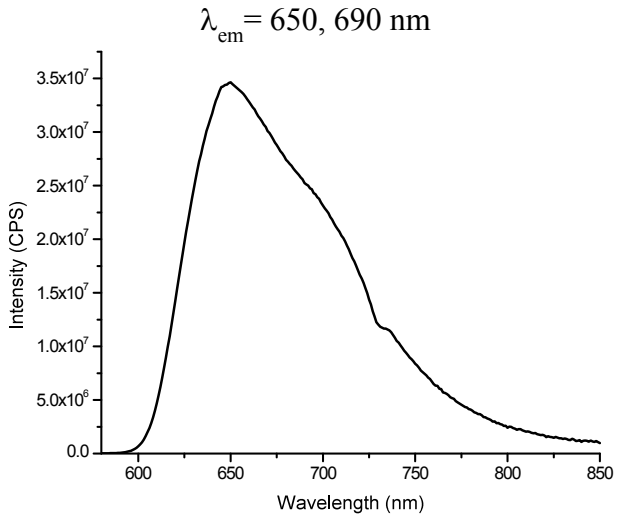

Figure S23. Emission spectrum of [{Ru(ttpy)}$_8$(**L^2**)](PF$_6$)$_{16}$ (**4**) in CH_3CN at 77 K.

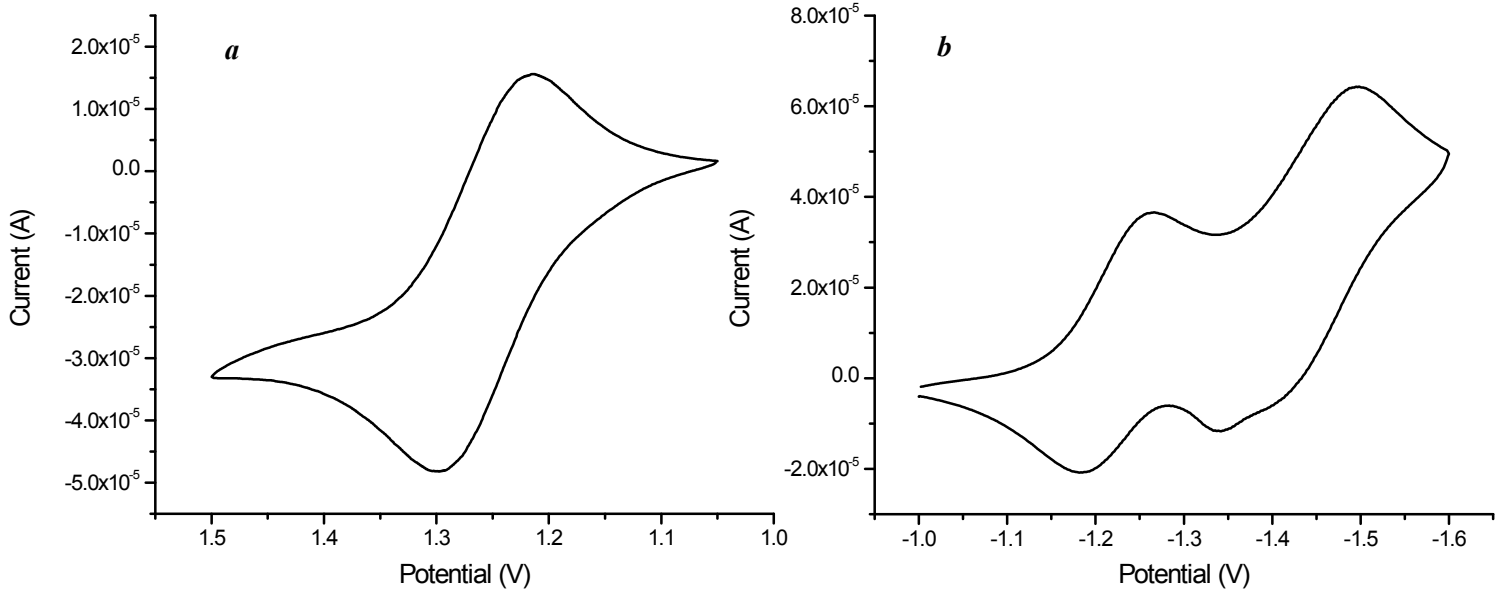

Figure S24. Cyclic voltammogram of $[\{Ru(ttpy)\}_8(\mathbf{L^2})](PF_6)_{16}$ (**4**) on a glassy carbon millielectrode in acetonitrile (0.1 M Et_4NClO_4) versus Ag/Ag^+ at 25 °C, scan rate = 50 mVs^{-1}, (a) positive potential and (b) negative potential window.